Research Paper

Repeated ultrasound treatment of tau transgenic mice clears neuronal tau by autophagy and improves behavioral functions

Rucha Pandit, Gerhard Leinenga and Jürgen Götz✉

Clem Jones Centre for Ageing Dementia Research, Queensland Brain Institute, The University of Queensland, St. Lucia, Brisbane, QLD 4072, Australia.

✉ Corresponding author: j.goetz@uq.edu.au

Abstract

Intracellular deposits of pathological tau are the hallmark of a broad spectrum of neurodegenerative disorders collectively known as tauopathies, with Alzheimer's disease, a secondary tauopathy, being further characterized by extracellular amyloid plaques. A major obstacle in developing effective treatments for tauopathies is the presence of the blood-brain barrier, which restricts the access of therapeutic agents to the brain. An emerging technology to overcome this limitation is the application of low-intensity ultrasound which, together with intravenously injected microbubbles, transiently opens the blood-brain barrier, thereby facilitating the delivery of therapeutic agents into the brain. Interestingly, even in the absence of therapeutic agents, ultrasound has previously been shown to reduce amyloid plaques and improve cognitive functions in amyloid-depositing mice through microglial clearance. Ultrasound has also been shown to facilitate the delivery of antibody fragments against pathological tau in P301L tau transgenic mice; however, the effect of ultrasound alone has not been thoroughly investigated in a tauopathy mouse model.

Methods: Here, we performed repeated scanning ultrasound treatments over a period of 15 weeks in K369I tau transgenic mice with an early-onset tau-related motor and memory phenotype. We used immunohistochemical and biochemical methods to analyze the effect of ultrasound on the mice and determine the underlying mechanism of action, together with an analysis of their motor and memory functions following repeated ultrasound treatments.

Results: Repeated ultrasound treatments significantly reduced tau pathology in the absence of histological damage. Associated impaired motor functions showed improvement towards the end of the treatment regime, with memory functions showing a trend towards improvement. In assessing potential clearance mechanisms, we ruled out a role for ubiquitination of tau, a prerequisite for proteasomal clearance. However, the treatment regime induced the autophagy pathway in neurons as reflected by an increase in the autophagosome membrane marker LC3II and a reduction in the autophagic flux marker p62, along with a decrease of mTOR activity and an increase in beclin 1 levels. Moreover, there was a significant increase in the interaction of tau and p62 in the ultrasound-treated mice, suggesting removal of tau by autophagosomes.

Conclusions: Our findings indicate that a neuronal protein aggregate clearance mechanism induced by ultrasound-mediated blood-brain barrier opening operates for tau, further supporting the potential of low-intensity ultrasound to treat neurodegenerative disorders.

Key words: Autophagy, blood-brain barrier, therapeutic ultrasound, protein aggregation disorders, tau

Introduction

Tauopathies are characterized by intracellular aggregates of the microtubule-associated protein tau in a hyperphosphorylated form [1]. Primary tauopathies, such as progressive supranuclear palsy

or corticobasal degeneration, present with a predominant tau pathology. Alzheimer's disease, in contrast, is a secondary tauopathy that is marked by the additional accumulation of amyloid-β aggregates as extracellular plaques, with tau forming neurofibrillary tangles (NFTs) [2, 3]. Under physiological conditions, tau is an unfolded and highly soluble protein that is enriched in the axon [4]. In tauopathies, tau becomes hyperphosphorylated and forms aggregates throughout the neuron in a fibrillar form [5]. The aggregation of hyperphosphorylated tau into NFTs is an ordered process [6], which may be driven by the *de novo* synthesis of tau in the cell body and dendrites [7]. There are currently no effective therapies for these disorders, as the current treatment of Alzheimer's disease with acetylcholinesterase inhibitors or the NMDA-receptor antagonist memantine provides only symptomatic relief. Although recent clinical trials are targeting the underlying biology of these disorders [8], a major challenge is the limited bioavailability of antibodies and other therapeutic agents in the brain, due to their incomplete passage across the blood-brain barrier (BBB) [9]. Here, the application of low-intensity ultrasound to transiently open this barrier is emerging as a potential therapeutic strategy [10], particularly given the successful application of ultrasound with microbubbles in humans in a phase I clinical study that established the safety of the protocol [11].

Focused ultrasound is a novel technology that uses acoustic energy to non-invasively target defined brain areas to treat disorders of the central nervous system [12]. At high intensity, this energy causes heating of the target tissue, with applications emerging in oncology by coagulating cancer tissue, and in movement disorders such as essential tremor and Parkinson's disease by lesioning thalamic tissue [13, 14]. At low intensity, in conjunction with gas-filled microbubbles which are routinely used as contrast agents, ultrasound can also transiently open the BBB, allowing for enhanced drug delivery into the brain [15, 16]. Opening of the BBB is achieved through an interaction between the microbubbles (which have a size in the low micrometer range) and the propagating sound wave, thereby causing the microbubbles to oscillate and the tight junctions of capillary endothelial cells to separate as a result of the downregulation of junction proteins, together with the upregulation of caveolae-forming proteins which leads to an increased trans-cytoplasmic transport [17]. Ultrasound has previously been applied to an Alzheimer's disease mouse model, opening the BBB at four locations in the right hemisphere to facilitate the delivery of an anti-amyloid-β antibody, which

achieved a reduction in plaque pathology [18]. A follow-up study showed a reduction of plaque area even in the absence of a therapeutic antibody [19]. Another study reported that bilaterally sonicating the hippocampus without administering any antibodies reduced amyloid plaque pathology and restored spatial working memory [20]. We used repeated low-intensity ultrasound in a scanning mode (scanning ultrasound, SUS) to open the BBB throughout the brain of mice with amyloid-β pathology; this treatment resulted in more than a twofold reduction in plaque pathology, accompanied by the restoration of memory functions in three behavioral tasks [21]. As a clearance mechanism, we identified the uptake of amyloid-β into the lysosomes of microglia, a process likely mediated by unidentified blood-borne factors that had entered the brain to activate the dormant microglia [21].

Despite an increasing number of studies using ultrasound to clear amyloid, the effect of ultrasound on tau has not been investigated in detail. In a previous study, we showed that just four ultrasound treatments to deliver a 2N tau isoform-specific antibody fragment reduced anxiety-like behavior and tau hyperphosphorylation in P301L tau-expressing pR5 mice when compared to a treatment with the antibody fragment alone [22]. This study also revealed a subtle reduction of hyperphosphorylated tau in the ultrasound only group, although the mechanism of reduction was not investigated, nor have the effects of ultrasound on a mouse model with tau-associated motor deficits been probed. Motor functions are important as the clinical spectrum of tauopathies includes not only syndromes with cognitive dysfunction, but also those with primary motor symptoms, including parkinsonism [23]. In this study, we investigated the effects of SUS treatments without any antibody intervention in the K3 mouse model. This mouse model harbors the K369I mutation of tau, presenting with prevalent NFTs in the cortex and hippocampus, as well as associated memory and locomotor defects [24]. In addition to this combined behavioral impairment, another advantage of this model is the early onset and robustness of tau pathology. Our results demonstrated that the K3 mice tolerate 15 weekly SUS treatments without overt histological damage. We found that repeated SUS treatments caused a significant reduction in tau phosphorylation, particularly in the hippocampus. It has previously been reported that tau can be cleared by stimulating autophagy [25]. We provide evidence that, following ultrasound, tau can also be removed by this process, demonstrating another ultrasound-mediated clearance mechanism in addition to the microglial activation previously reported for

amyloid-β [21]. In addition to the histological improvements, we also saw an improvement in motor and a tendency towards improvement in memory functions, supporting the notion that ultrasound is a promising treatment option for Alzheimer's disease and possibly other aggregation disorders.

Materials and methods

Animals

K3 mice expressing the K369I mutation of tau under the control of the mThy1.2 promoter have been described previously [24]. Age- and gender-matched K3 mice and non-transgenic littermates were used for this study (n=20 each). The animals were housed in specific pathogen-free cages and maintained on a 12 h light/dark cycle, with constant access to food and water. An equal number of male and female K3 mice were randomly assigned to the SUS and sham control groups (total of 10 animals per group). Animal experimentation was approved by the Animal Ethics Committee of the University of Queensland (approval number QBI/412/14/NHMRC).

SUS equipment

An integrated focused ultrasound system with a center frequency of 1 MHz was used as previously detailed (Therapy Imaging Probe System, TIPS, Philips Research) [26]. The system consisted of an annular array transducer having a natural focus of 80 mm, with an 80mm radius of curvature, housed in an 80mm spherical shell with a central opening of 31 mm diameter, a 3D positioning system, and a programmable motorized system to move the ultrasound focus in the x and y planes to cover the entire brain. A coupler mounted to the transducer was filled with degassed water and placed on the head of the mouse with ultrasound gel for coupling, to ensure propagation of the ultrasound to the brain. The focus of the transducer had dimensions of 1.5 × 12 mm in the transverse and axial planes, respectively.

Production of microbubbles

In-house prepared microbubbles comprising a phospholipid shell and octafluoropropane gas core were used. 1,2-distearoyl-*sn*-glycero-3-phospho-choline (DSPC) and 1,2-distearoyl-*sn*-glycero-3-phosphoethanolamine-N- [amino (polyethylene glycol)-2000] (DSPE-PEG2000) (Avanti Polar Lipids) were mixed at a 9:1 molar ratio dissolved in chloroform (Sigma) and the chloroform solvent was evaporated under vacuum. The dried phospholipid film was then dissolved in phosphate-buffered saline (PBS) with 10% glycerol to a concentration of 1 mg lipid/ml and heated to 55°C in a sonicating water bath. The solution was placed in 1.5 ml glass HPLC vials and the air in the vial was replaced with octafluoropropane (Arcadophta). On the day of the experiment, individual vials were agitated in a dental amalgamator at 4,000 rpm for 45 s to generate the microbubbles. Microbubbles were observed under a microscope to be polydispersed and under 10 μm in size at a concentration of $1–5 × 10^8$ microbubbles/ml.

SUS application

The mice were anesthetized with ketamine (90 mg/kg) and xylazine (6 mg/kg) and the hair on the head was shaved and depilated. The animals were then injected intravenous retro-orbitally with 1 μl/g body weight of microbubble solution and then placed under the ultrasound transducer with the head immobilized. We have previously found that retro-orbital injections give identical results to tail vein injections and are technically easier to perform. Ultrasound gel was used to seal all interfaces to eliminate air gaps. Parameters for the ultrasound delivery were 0.65 MPa peak rarefactional pressure, 10 Hz pulse repetition frequency, 10% duty cycle, and a 6 s sonication time per spot. The motorized positioning system moved the focus of the transducer array in a grid with 1.5 mm spacing between individual sites of sonication so that ultrasound was delivered sequentially to the entire brain. Mice typically received a total of 24 spots of sonication in a 6 × 4 raster grid pattern. For sham treatment, mice received all injections and were placed under the ultrasound transducer, but no ultrasound was emitted. SUS and sham treatments commenced at 6 weeks of age, and were performed once every week for 15 weeks.

Tissue processing

72 h after the final SUS treatment (week 20), the mice were anesthetized and perfused with 30 ml PBS. The brains were dissected and then separated into two hemispheres. The right hemisphere was fixed in 4% paraformaldehyde for 24 h, and then embedded in paraffin wax, with 10 μm coronal sections obtained on a microtome. The left hemisphere was further dissected to separate the cortex, hippocampus, cerebellum and remaining tissue, and then snap frozen in liquid nitrogen and stored at -80°C for further processing.

Immunohistochemistry

Paraffin-embedded coronal brain sections (between Bregma -1.34 and -2.06 mm) were analyzed immunohistochemically as previously described [24], using at least four sections per animal. For the wild-type group, 10 mice (5 of each gender) were picked randomly for assessment. Tau immunoreactivity was probed with the AT8 antibody

(1:500, Thermo Scientific), using a biotin-coupled anti-mouse secondary antibody (1:500), followed by detection with the ABC-HRP detection kit (VectaStain) and metal-enhanced 3,3'-diaminobenzidine (DAB, Dako) staining, and counterstaining with hematoxylin (Dako). The mean percentage area of tau positivity was calculated based on the areas which had a DAB intensity more than three standard deviations higher than the mean DAB intensity for wild-type animals, which lack a tau pathology. Bielschowsky staining and analysis of NFT- like inclusions were performed as previously described [24, 27]. NFTs were manually counted in ImageJ when stained dark brown or black. For immunofluorescence, a newly synthesized antibody against pS235-tau, RN235, was used (1:5,000, in-house, now available from Merck as MABN2275) [28]. For detection, a goat anti-mouse AlexaFluor 488 secondary antibody (1:500) was used, together with the nuclear stain 4', 6-diamidino-2-phenylindole (DAPI, 1: 10,000), and the number of positive puncta in the entire hippocampus and cortex were counted. All images were obtained on an automated slide scanner microscope (Zeiss) at 20X magnification. Image quantification and analysis were performed blinded using ImageJ software (NIH).

To investigate autophagy, brain sections were stained for the autophagy marker p62 (anti-SQSTM1) (mouse, 1:500, Abcam). Goat anti-mouse AlexaFluor 488 secondary antibody (1:500) was used for detection. A no-primary antibody control was used to set the threshold for analysis. For quantification, particles over $0.1\mu m^2$ were measured using ImageJ, which was also used to assess the size distribution. To determine cellular identity, p62 (mouse, 1:500, Abcam) was visualized together with either the neuronal marker MAP2 (chicken, 1:2,000, Abcam), or the microglial marker Iba1 (rabbit, 1:500, Wako), and the astrocytic marker GFAP (goat, 1:500, Santa Cruz) on serial sections (due to secondary antibody restraints), and then detected with anti-mouse AlexaFluor647, anti-chicken AlexaFluor488, anti-rabbit AlexaFluor488 and anti-goat AlexaFluor594 secondary antibodies, respectively. All images were obtained at 63X magnification on a Zeiss 710 confocal microscope and analyzed using ImageJ software.

Sequential protein extraction

Sequential protein extraction was performed on tissue dissected from the left hemisphere. Briefly, the cortex and hippocampus were dissolved in 6X and 10X (w/v) RAB buffer, respectively, containing 10 mM sodium fluoride, 1 mM sodium orthovanadate, 1 mM phenylmethylsulfonyl fluoride, and complete protease inhibitor (Roche), together with a phosphatase inhibitor cocktail (Invitrogen). The tissue was dissociated using a tissue lyzer for 6 min for the cortex, and using a syringe with a 27-gauge needle for the hippocampus, followed by a brief sonication step, and centrifuged at 21,000g for 90 min to extract the extracellularly enriched fraction. The pellet was homogenized in the same volume of RIPA buffer containing the aforementioned inhibitors and was again centrifuged at 21,000g for 90 min to obtain the intracellular, detergent-soluble fraction. The protein concentration of the fractions was determined using the BCA assay (Pierce). All extraction steps were performed at 4°C and the aliquots and final pellets were stored at -80°C until further use.

Western blotting

20 µg each of the extracellularly enriched and the detergent-soluble fraction were separated on a 10% SDS-PAGE gel and then transferred onto a 0.45 µm low-fluorescence polyvinylidene difluoride membrane using Turbo Transfer buffer (Bio-Rad). The number of wells restricted the samples analyzed per gel, and male and female mice were run on separate gels. Eight wild-type mice and 10 SUS-treated and 10 sham mice were used for the analysis. To visualize tau, the membranes were blocked in Tris-buffered saline (TBS) containing Odyssey Blocking Buffer (Li-Cor), and incubated overnight in a 1:2,000 dilution of AT8 (Thermo Scientific). Rabbit anti-GAPDH antibody (1:5,000; Millipore) was used as an internal loading control. The membranes were then probed with anti-mouse IgG (IR800) and anti-rabbit IgG (IR680) secondary fluorescence antibodies (1:10,000; Li-Cor) and imaged on the Li-Cor Odyssey scanner. Signals from the detected bands were quantified using the Image Studio software (Li-Cor). The intensities were normalized to GAPDH for quantification.

For elucidation of potential mechanisms, primary antibodies against phosphorylated glycogen synthase kinase β (pGSK3β) and GSK3β [for kinase activity (rabbit, 1:1,000, CST)], and against LC3 (rabbit, 1:2,500, CST) p-mTOR (rabbit, 1:500, CST), mTOR (rabbit, 1:500, CST), Beclin 1 (rabbit, 1:500, CST) and Atg12 (rabbit, 1:500, CST) [for autophagy] were used with GAPDH (mouse, 1:5,000) as an internal loading control. Secondary antibodies were used as described above.

Proximity ligation assays

To detect the presence of tau in autophagosomes, we performed the proximity ligation assay (PLA) using an anti-tau antibody and an anti-p62 antibody as the primary pair, followed by detection with Duolink reagents (Duolink *In Situ* Detection Reagents

Orange, DUO92007, Sigma) as per the manufacturer's instructions. Briefly, paraffin-embedded brain sections were rehydrated, followed by antigen retrieval in citrate buffer (pH 5.8) and then blocked in blocking buffer. These sections were incubated overnight with rabbit anti-tau antibody (1:1000, Dako) and mouse anti-p62 antibody (1:500, Abcam). The same rabbit anti-tau antibody was paired with a mouse anti-α tubulin monoclonal antibody (1:500, Sigma) as a positive control, whereas for the negative control no primary antibodies were used. PLA probes (anti-mouse and anti-rabbit) were applied, followed by ligation and amplification as per the standard protocol. DAPI was used as the nuclear marker and the sections were imaged at 63X magnification on a Zeiss LSM 510 confocal microscope. For quantification, the no-primary antibody negative controls were used to set the threshold, and a positive signal was measured as any particle over $0.1\mu m^2$ in size. Image analysis was performed using ImageJ software.

Behavioral tests

The weight of all animals (20 wild-type, 10 SUS-treated and 10 sham-treated mice) was monitored weekly. For the repeated Rotarod paradigm to test motor function, mice were habituated to the experimental room for at least 30 min before the test. Illumination was kept constant at 60% (~70 Lux) throughout the period of testing. Animals were then tested on the Rotarod in acceleration mode (4 to 40 rpm) over 90 s with the total test time being 180 s (90 s at 40 rpm). The longest time a mouse remained on the rod out of 3 attempts was recorded as its latency to fall, for each week throughout the course of the treatment. In order to assess grip strength, mice were allowed to grasp a metal T-bar and the average peak force out of 10 trials to release the metal bar was measured.

The Y-maze test was used to assess spatial working memory. The maze was made of transparent Plexiglas with three identical arms (40 x 9 x 16 cm) positioned 120° apart. Mice were habituated to the experimental room and the maze for 4 min, 60 min before the test. Illumination was kept constant at 60% (~70 Lux) throughout the test period. At the time of testing, the mice were placed in an arm of the maze and allowed to explore the entire maze for 8 min, while being videotaped. The percentage alternation between arms A, B and C was calculated by the number of complete alternation sequences (i.e., ABC, BCA, CAB) divided by the number of alternation opportunities (total arm entries minus two). An arm entry was recorded when the animal had all four paws inside the arm.

The novel object recognition (NOR) test was used to assess short-term memory, which relies on the natural instincts of rodents to explore novel objects more than familiar ones. Due to the non-availability of the test apparatus during week 15, there was one cohort of mice that could not be tested to adhere to the weekly ultrasound protocol. This resulted in the testing of 17 wild-types, 8 SUS-treated mice and 7 sham-treated mice. This number was kept the same for week 19 to avoid confounding the results. Mice were habituated to the room as well as to two identical objects placed in a white box (30.5 x 30.5 cm) for 8 min at 60% illumination. After 60 min, one of the objects was replaced with a novel object and the mice were allowed to explore the objects for 4 min, while being videotaped. The time the mice spent exploring the novel object, defined as exploration with the nose less than 1 cm from the object, was measured with Ethovision software.

Statistical analysis

Statistical analysis was performed on Prism7 (GraphPad Software) using one-way ANOVA and Tukey's multiple comparison tests, and a two-way ANOVA to analyze the results of the Rotarod test. All values are expressed as mean ± SEM, unless otherwise specified.

Data availability

Raw data were obtained and analyzed at the University of Queensland. Data supporting the finding of this study are available from the corresponding author on request.

Results

Repeated ultrasound treatment reduces hyperphosphorylated tau and neurofibrillary tangles

The impact of repeated SUS treatments on the entire brain were explored in the K369I tau transgenic K3 mouse model that is characterized by an NFT-like tau pathology and pronounced associated memory and motor impairment [24, 27]. The transgenic mice were randomly assigned to two groups, with the treatment group (SUS) receiving weekly SUS treatments (microbubbles plus ultrasound under anesthesia) over 15 weeks, initiated at 6 weeks of age, whereas the control group (sham) received the microbubbles under anesthesia, without ultrasound application. A third group of age-matched wild-type littermates was used as a control for (normal) cognitive and motor functions and was not subjected to any treatments (Figure 1). At the end of the test period, the mice were sacrificed for immunohistochemical and biochemical analysis.

Hyperphosphorylation of tau at specific serine and threonine residues has been implicated in tau aggregation, the spread of pathology and neurodegeneration in Alzheimer's disease [29]. We therefore assessed the effect of SUS on tau immunohistochemically and biochemically, using a phospho-tau-specific antibody, AT8, which detects tau phosphorylation at Ser202/Thr205. At the age of sacrifice (20 weeks), AT8 staining was pronounced in the CA2/CA3 region of the hippocampus and dispersed across the entire cortex in the sham group (Figure 2A). In comparison, SUS treatment resulted in a 3-fold reduction in AT8-positive tau deposits in the hippocampus (Figure 2B), whereas no significant effect was observed in the cortex (Figure 2C). However, it should be noted that for the cortex, the pathology was dispersed across the entire tissue rather than being confined to a specific region as in the hippocampus, which may have diluted the effects observed. The K3 mouse model also presents with a very subtle tau pathology in the cerebellum due to the choice of promoter for transgene expression, which is why we assessed AT8 phosphorylation in this region as an additional control since we had not targeted the tissue with SUS and found no differences between the SUS- and sham-treated mice (Figure S1). Because tau pathology in the K3 mice is progressive and tau deposition results in Bielschowsky silver-positive NFT-like neuronal inclusions, we analyzed the number of these inclusions following ultrasound treatments in the hippocampus and the cortex. We observed a significant reduction of the number of NFT-like inclusions in the SUS-treated mice as compared to the sham group (Figure S2). Although Bielschowsky staining revealed a reduction of NFT-like inclusions in the SUS-treated mice, it also yielded high background staining. We therefore used the late-stage NFT-specific antibody RN235 that is specific for tau phosphorylated at S235 [28]. This revealed a two-fold reduction in the number of NFTs

in the SUS compared to the sham group in both the hippocampus and the cortex (Figure 2D-F).

Next, we analyzed the levels of total and insoluble phospho-tau species in lysates obtained from dissected hippocampi and cortices that had undergone sequential extraction in RAB (more soluble) and RIPA (insoluble proteins) buffer (Figure 2G). Data are only shown for the RIPA fractions as there was no change in the RAB fractions. The AT8 antibody revealed a trend towards a reduction in phosphorylated tau in the hippocampus (p=0.0769, Figure 2H), which was not observed in the cortex (Figure 2I). The lack of significance in the biochemical analysis could be because of the dilution of the signal due to the heterogeneity of the cells with regards to treatment effects or transgene expression when compared to immunohistochemistry, which provides a cellular resolution. However, given the observation of reduction in hyperphosphorylated tau in our immunohistochemical or a similar trend thereof in biochemical analysis, we conclude that repeated SUS treatments reduce hyperphosphorylated tau in K3 mice.

Repeated ultrasound treatment induces autophagy-mediated clearance of tau

Hyperphosphorylation of tau at various serine and threonine residues has been implicated in tau aggregation, which in turn is a prerequisite for neurodegeneration. Having revealed a reduction in phosphorylation following repeated SUS treatments in the hippocampus, we next assessed the activity of the major serine and threonine kinase that phosphorylates tau at the AT8 and RN235 epitopes – GSK3β. This analysis did not detect any significant difference in kinase activity (determined using total and pSer9-GSK3 antibodies) in the hippocampus (RAB fraction, Fig S3). Given that hyperphosphorylated tau was significantly reduced in the hippocampus of the SUS group, we therefore addressed alternative mechanisms.
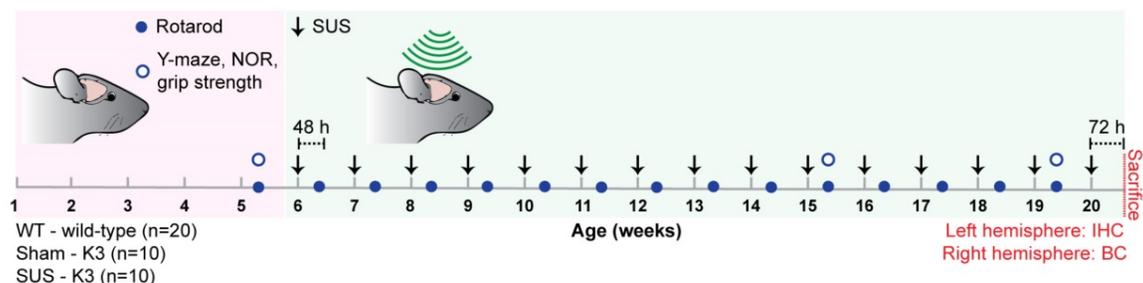

Figure 1. Repeated scanning ultrasound treatment scheme for K3 mice including behavioral tests and *post mortem* analysis. Study design for ultrasound treatments involving three groups of mice – scanning ultrasound (SUS)- and sham-treated K3 mice (n=10 for each group) and wild-type (WT) littermate controls (n=20). SUS and sham treatments (arrows) were initiated at 6 weeks of age, and performed once every week for 15 weeks (green shaded area), with Rotarod performance (closed blue circles) being monitored 48 h after every treatment as a measure of efficacy. Memory function (Y-maze and novel object recognition, NOR) and grip strength (open blue circles) were assessed at weeks 5 (baseline, red shaded area), 15 and 19. Mice were sacrificed at 20 weeks of age, 72 h after the last SUS or sham treatments for further immunohistochemical (IHC) and biochemical (BC) tests.
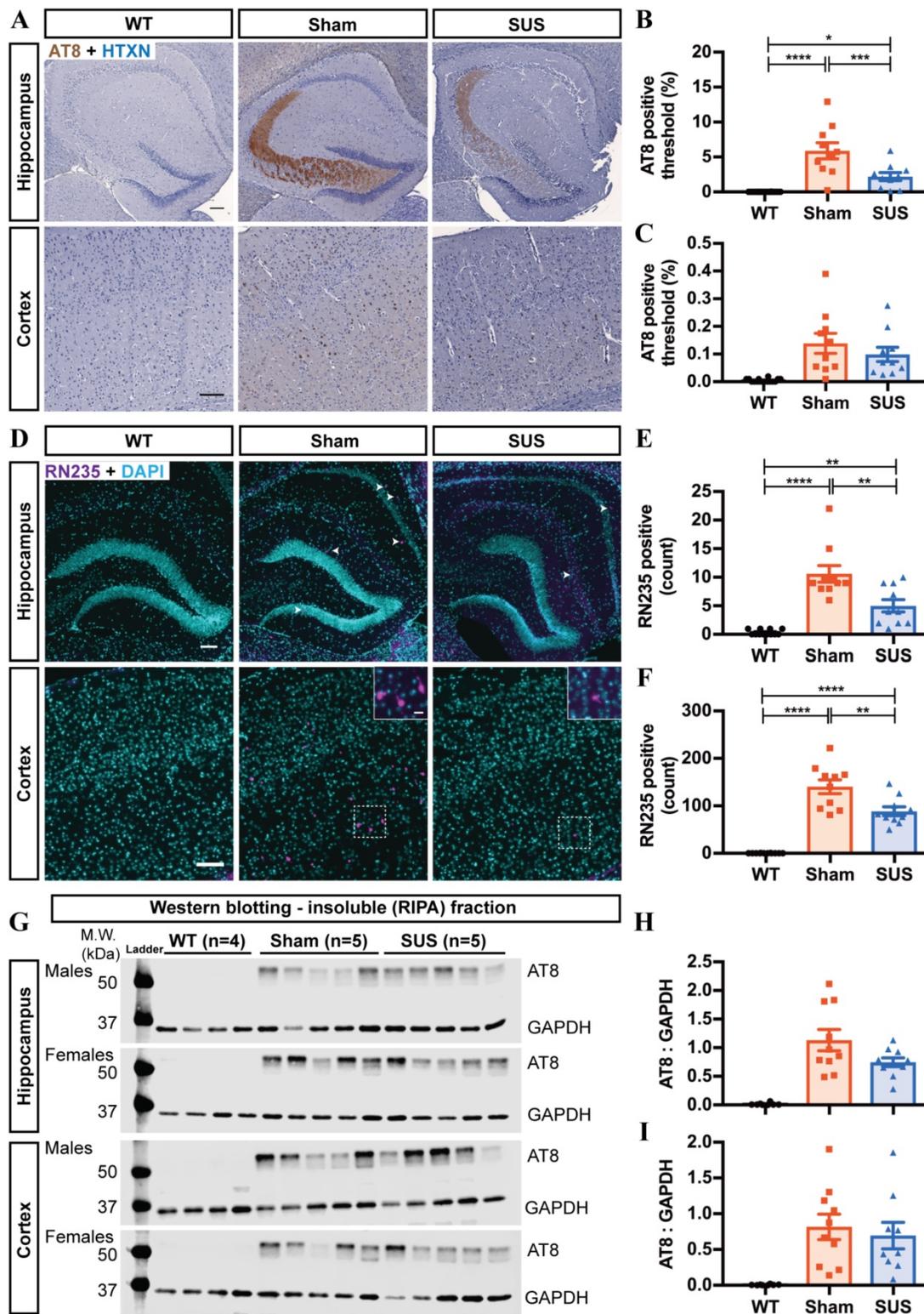
Figure 2. Repeated ultrasound treatments reduce both early- and late-stage hyperphosphorylated tau. (A) Phosphorylation at the AT8 epitope of tau (Ser202/Thr205) was detected in both the cortex and the hippocampus of K3 animals (n=10 WT, 10 sham and 10 SUS-treated mice) Scale bar: 100 μm. (B) Phosphorylation at the AT8 epitope was markedly reduced in the hippocampus of the SUS versus the sham group, whereas no staining was observed in WT mice (one-way ANOVA with Tukey's multiple comparison test, *p<0.05, ***p<0.001, ****p<0.0001). (C) No significant difference was found for the cortex (2 WT outliers excluded). (D) Staining with the pSer235-specific antibody RN235 revealed NFT-like inclusions in both the sham- and SUS-treated mice in the hippocampus (arrowheads) and the cortex (n=10 WT, 10 sham and 10 SUS-treated mice). Scale bar: 100 μm (inset, scale bar: 20 μm). Quantification of the RN235-positive inclusions in (E) the hippocampus and (F) the cortex demonstrated a significant reduction in the SUS-treated mice as compared to the sham controls. (one-way ANOVA with Tukey's multiple comparison test, **p<0.01, ****p<0.0001). (G) Tau was sequentially extracted to yield the (RIPA) insoluble fractions from the hippocampus and the cortex (n=8 WT, 10 sham and 10 SUS-treated mice). Staining with the AT8 antibody revealed a trend towards decreased phosphorylation in (H) the hippocampal fractions (p=0.0769), but not in (I) the cortical fractions. (one-way ANOVA with Tukey's multiple comparison test) (1 SUS-treated outlier excluded).

Accumulation of hyperphosphorylated tau can occur due to an increase in synthesis and enzymatic activity, as well as a failure in clearance [30]. In assessing amyloid clearance mediated through ultrasound, we had previously demonstrated a role for microglia in the phagocytosis of amyloid-β plaques [21, 31]. Microglia are the resident immune cells in the brain, and are thought to play an important role in clearing extracellular tau. When assessing SUS- compared to sham-treated K3 mice, we noted an increase in the number of activated microglia following ultrasound treatment. However, as we failed to visualize any extracellular tau or tau co-localizing with the microglial lysosomal marker CD68 in the K3 mice, we explored other potential mechanisms of tau clearance. Whereas tau in its normal state is effectively cleared through proteasomal degradation, a number of studies have highlighted a possible impairment of the proteasome in degrading aggregated tau, as well as a role for autophagosomes in mediating this degradation [reviewed in [32]]. We therefore assessed the proteasomal and autophagosomal pathways in the SUS and sham groups. As proteins degraded by the proteasome are ubiquitinated, we immunoprecipitated tau from the hippocampal lysates of the SUS and sham mice and probed it for ubiquitination. This analysis did not reveal any significant differences in ubiquitinated tau levels between the two groups, nor did we observe any general increase in protein ubiquitination following SUS treatment (Figure S4).

We next investigated the effect of repeated SUS treatment on the autophagy pathway by analyzing the protein markers LC3 and p62. LC3 is conjugated to phosphotidylethanolamine to form LC3II, which is the lipidated form of LC3 and localizes to autophagosomes and therefore reflects the number of autophagosomes and autophagy-related structures. While we found no difference in the levels of LC3II in the RAB fractions obtained from either the hippocampus or the cortex (data not shown), the hippocampal RIPA fractions exhibited a trend towards an increase in the lipidated form of LC3II in the SUS group compared to the sham controls (p=0.0804, Figure 3A, B). This difference was not observed in the cortical RIPA lysates (Figure 3C). To definitively demonstrate that ultrasound induces autophagy, we investigated other important proteins in the autophagic pathway and the formation of the autophagosome. We first looked at the activity of mammalian target of rapamycin (mTOR), a Ser/Thr kinase. The activity of mTOR negatively regulates autophagic machinery and autophagosome initiation. We observed a significant reduction of mTOR activity

(p-mTOR/mTOR) in the SUS-treated mice as compared to the sham group (Figure 3D, E) We also investigated the levels of beclin 1, the mammalian ortholog of yeast Atg6, which plays a role in autophagosomal nucleation [33] and found that it was significantly increased in the SUS-treated mice as compared to the sham mice (Figure 3F, G). In contrast, there was no difference in the amount of Atg12-Atg5 conjugate, which is required for autophagosome elongation and facilitates the lipidation of members of the LC3 family [34], between the SUS-treated and sham mice (Figure 3H, I). We next probed p62 as a marker for autophagic flux [35], given that this protein acts as a receptor which directly binds to LC3 and is selectively degraded by autophagy [36]. Staining of brain sections with the p62 antibody (Figure 3J) revealed a significant reduction in the number of p62-positive puncta in the hippocampus of the SUS-treated when compared to the sham hippocampus (Figure 3K). There was also a change in the size distribution of the puncta, with the SUS-treated mice having smaller puncta similar to those found in wild-type mice, in contrast to the sham mice which had larger puncta (Figure 3L). This reduction in the number and size of the puncta suggested an induction of autophagy as p62 accumulates and forms larger puncta when autophagy is inhibited and is reduced when autophagy is induced [37]. We next investigated the cell-type in which autophagy was induced in the SUS-treated K3 mice. Staining brain sections for p62 together with neuronal or glial markers revealed a significant co-localization of the p62 signal with the neuronal marker MAP2, but not with the astrocytic marker GFAP or the microglial marker Iba1 (Figure S5). The data were quantified based on the intensity of the p62 signal obtained from either neurons (MAP2-positive areas) or glia (Iba1- and GFAP-positive areas). The increase in the amount of lipidated LC3, decrease in mTOR activity and increase in beclin 1, together with the decrease in the intraneuronal localization of p62 staining, indicates an increase in autophagic activity in the neurons of the SUS-treated K3 mice, rather than in their glia.

In order to further visualize the degradation of tau in the autophagosomes, we performed a proximity ligation assay (PLA) for tau and p62. In this assay a close interaction between two proteins of interest generates a signal that can be detected in brain sections (Figure 4A). Our analysis revealed that SUS treatment led to a two-fold increase in the PLA signal in the hippocampus, as compared to the sham treatment (Figure 4B, C). As a positive control, we made use of the known interaction between tau and tubulin, which gave a strong positive signal, whereas

the negative control omitting the primary antibody yielded no signal (Figure 4C). These results indicate that repeated ultrasound treatments lead to an increased degradation of tau via autophagy.
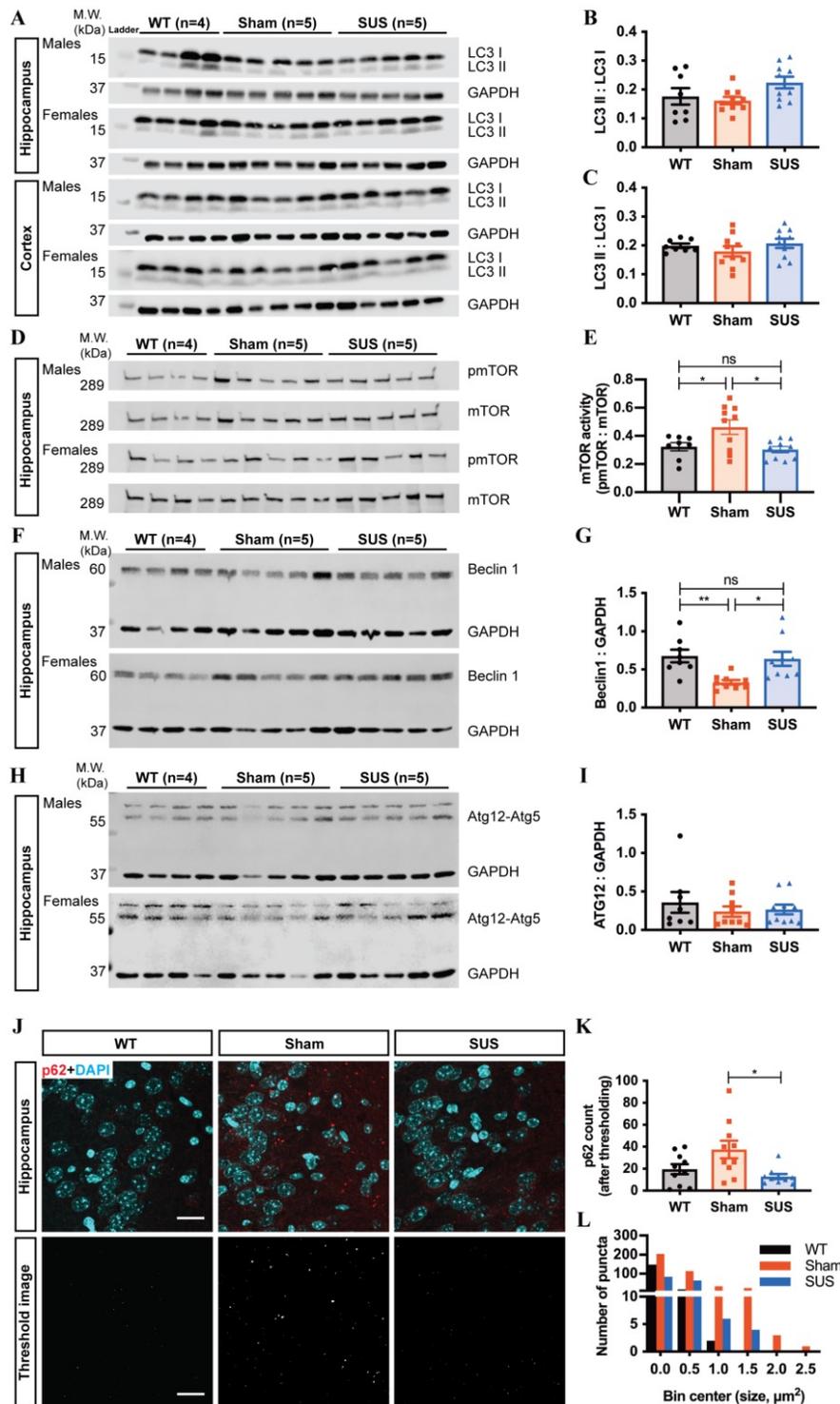

Figure 3. Repeated ultrasound treatments induce autophagy in neurons. (A) LC3 II levels in the hippocampal and cortical insoluble fractions were analyzed by western blotting (n=8 WT, 10 sham and 10 SUS-treated mice). (B) This analysis revealed a trend towards increased lipidated LC3 II in the SUS mice compared to the sham group (one-way ANOVA with Tukey's multiple comparison test, p=0.0804). (C) No significant difference in the level of LC3 II was observed in the cortical fractions. (D) Activity of the kinase mTOR was analyzed in the hippocampal RAB fractions as a ratio of phospho-mTOR (pSer2448) to mTOR, revealing (E) a significant reduction of mTOR activity in the SUS mice as compared to the sham group (one-way ANOVA with Tukey's multiple comparison test, *p<0.05). (F) Beclin 1 levels in the hippocampal insoluble fractions were analyzed (n=8 WT, 10 sham and 10 SUS-treated mice) and (G) were found to be significantly increased in the SUS-treated animals as compared to the sham mice (one-way ANOVA with Tukey's multiple comparison test, *p<0.05, **p<0.01) (1 SUS- and 1 sham-treated outlier excluded). (H, I) No significant difference in the level of the Atg12-Atg5 conjugate complex was observed in the hippocampal fractions between the three groups (one-way ANOVA with Tukey's multiple comparison test). (J) Staining with the p62 antibody revealed (K) a significant reduction of the number of p62 puncta in the SUS-treated mice compared to the sham group (one-way ANOVA with Tukey's multiple comparison test, *p<0.05) (n=10 WT, 10 sham and 10 SUS-treated mice). (L) Change in the distribution of p62-positive puncta (green) in the SUS mice compared to the sham group, with the SUS mice having smaller diffuse puncta. Scale bar: 20μm.
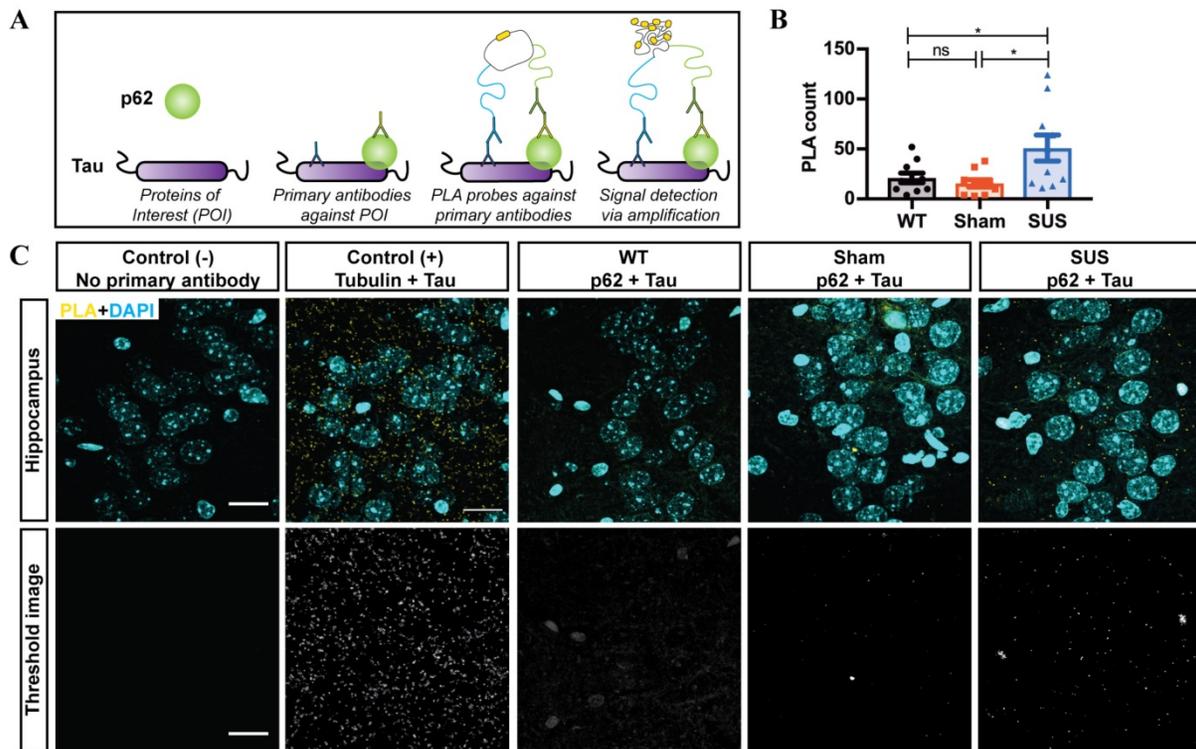
Figure 4. Repeated ultrasound treatments could potentially mediate neuronal tau clearance. (A) Graphical representation of the proximity ligation assay (PLA) between tau and p62. (B) Quantification of the positive PLA signal between tau and p62 revealed a significant increase in the SUS-treated mice as compared to the sham and WT mice (one-way ANOVA with Tukey's multiple comparison test, *p<0.05) (n=10 WT, 10 sham and 10 SUS-treated mice) (C) For the PLA experiment, the interaction between tau and tubulin was used as a positive control (+), no antibody was used as a negative control (-), and the interaction between tau and p62 was measured for all three experimental groups. Scale bar: 20 μm.

Taken together, our data suggest that the observed reduction in phosphorylated tau following repeated ultrasound treatments is, at least in part, mediated by the increased clearance of intracellular tau species through autophagy in affected neurons.

Repeated ultrasound treatments improve locomotor function in tau transgenic K3 mice

As K3 mice display a tau-dependent motor impairment as early as 5 weeks of age (Figure 5A), their performance was monitored on the Rotarod at week 5 and then again 48 hours after every sonication in order to assess motor ability and coordination, a readout of treatment outcome. The Rotarod was operated in an acceleration mode and the maximum latency for the mice to fall from the rod, out of 3 repeats, was measured. In the course of ultrasound treatment, mice in all three groups showed a variation in their latency to fall from the Rotarod (Figure 5B-D). However, the variation among the mice in the SUS group was higher (Figure 5D), when compared to that of the sham group (Figure 5C). More importantly, in the second half of the treatment period (from week 11 onwards), several SUS-treated mice performed considerably better than sham controls and almost as well as wild-type mice. A two-way ANOVA revealed a significant column effect of treatment between the

sham and SUS-treated mice. Tukey's multiple comparisons test found that K3 SUS-treated mice spent significantly more time on the Rotarod on average (70.92 seconds) than K3 sham-treated mice (55.67 seconds), when averaged over all the days. The average performance of the SUS group on the Rotarod started to diverge from that of the sham group from week 12, with the difference being statistically significant at weeks 15 and 16 of age (i.e. after 10 SUS treatments) (Figure 5E). Because the performance of mice on the Rotarod is determined by motor coordination and learning, as well as limb strength, we also compared the grip strength between the sham and SUS groups at week 15 (Figure 5F) and at the end of the study at week 19 (data not shown). However, we found no difference, suggesting that the improvement mediated by SUS treatment is at the level of coordination rather than muscle strength.

As this was the first study in which mice were subjected to weekly ultrasound treatments for such a long duration, and because K3 mice show a reduced body weight gain compared to wild-type mice [24, 27], we also monitored the weight of the animals throughout the study and found that, although both the SUS and sham K3 groups showed less weight gain than wild-type mice, there was no difference between the sham and SUS groups at any time-point (Figure S6
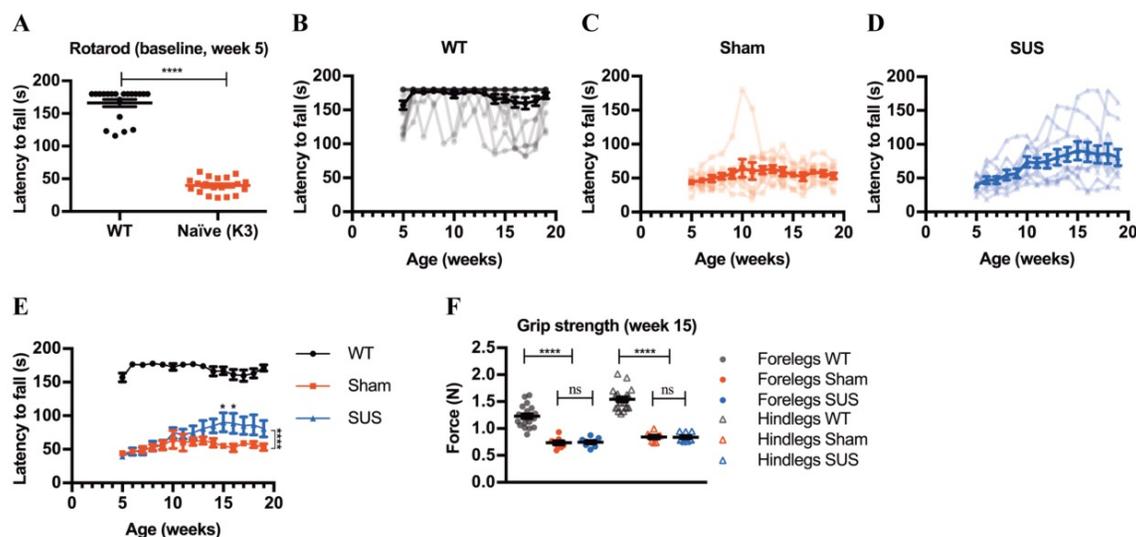
Figure 5. Repeated scanning ultrasound treatments improve motor functions of K3 mice. (A) Naïve K3 mice had a significantly lower latency to fall from the Rotarod at 5 weeks of age compared to WT mice (two-tailed unpaired *t*-test, ****$p<0.0001$) (n=20 WT and 20 K3 mice). The performance of individual mice (opaque symbols and lines) and the mean (solid symbols and line) over the course of the treatment was plotted for (B) WT (n=20), (C) sham-treated K3 (n=10) and (D) SUS-treated K3 (n=10) groups, revealing variation within each group throughout the duration of the study. (E) The mean latency to fall from the Rotarod for all three groups at each time point was plotted (WT: black circles, sham: red squares and SUS: blue triangles). A two-way ANOVA revealed a significant effect of treatment [$F_{(2, 40)} = 79.82$, ****$p<0.0001$]. A Tukey's multiple comparisons test found that K3 SUS-treated mice spent significantly more time on the rotarod on average (70.92 s) than K3 sham-treated mice (55.67 s), when averaged over all the days (****$p<0.0001$). The performance of the SUS and sham groups deviated from week 12 onwards and was significantly different at weeks 15 and 16 (two-way ANOVA with Tukey's multiple comparison test, *$p<0.05$). (F) The grip strengths of the hind- and forelimbs measured at week 15 were similar for the sham and SUS groups, but remained significantly lower than those of their WT littermates (one-way ANOVA with Tukey's multiple comparison test, ****$p<0.0001$).

A, B). Although the K3 mice had reduced body weight, there was no difference between the weights of the cortices and hippocampi between the SUS-treated and sham K3 mice, and the wild-type littermates (Figure S6 C, D). As a readout of the safety of the procedure, we also found no significant change in the number of damaged neurons or hemorrhages in either the hippocampus or the cortex between the sham and SUS groups when they were analyzed *post mortem* (Figure S6 E-G). Together, these findings indicate that the 15 ultrasound treatments were safely tolerated by the K3 mice, leading to improved motor function.

Repeated ultrasound treatments may improve memory functions in K3 mice

K3 mice display deficits in spatial working memory which become evident from 4 months of age onwards [24]. To investigate spatial working memory, the percentage of spontaneous alternations was calculated in the Y-maze (Figure 6A). Naïve K3 mice did not show any memory impairment at week 5 (Figure 6B). However, following repeated ultrasound treatments, the SUS group performed significantly better than the sham group, performing spontaneous alternations about 65% of the time at both weeks 15 (Figure 6C) and 19 (Figure 6D), whereas the sham group alternated approximately 55% of the time. Although we saw a significant improvement in the SUS-treated mice, we could not neglect the fact that the K3 sham mice did not show any impairment

compared to their wild-type littermates at either of the timepoints tested. This led us to test recognition memory in the NOR paradigm (Figure 6E), which is a more robust measure of memory function. Again, the naïve animals did not show any memory impairment at week 5, preferring to explore the novel object more than the familiar one (Figure 6F). Following SUS there was no significant difference between the groups, although the SUS group showed a trend towards increased exploration of the novel object (average 60%), whereas the sham group did not display any such preference at either week 15 (Figure 6G) or 19 (Figure 6H) (average 40%). Exploration times were normalized to the total movement of each mouse to avoid confounding effects of differences in motor function. Together these data indicate that repeated SUS treatment of K3 mice may improve some aspects of memory function.

Discussion and conclusions

Primary tauopathies are characterized by the aggregation and propagation of hyperphosphorylated, insoluble and filamentous tau [1], whereas Alzheimer's disease is a secondary tauopathy with amyloid-β plaques in addition to tau-containing NFTs. The use of low-intensity ultrasound in conjunction with microbubbles to transiently open the BBB has been shown to reduce amyloid-β pathology in a range of mouse models [19, 21]. This approach has also been used to deliver an anti-tau therapeutic to a mouse model with tau
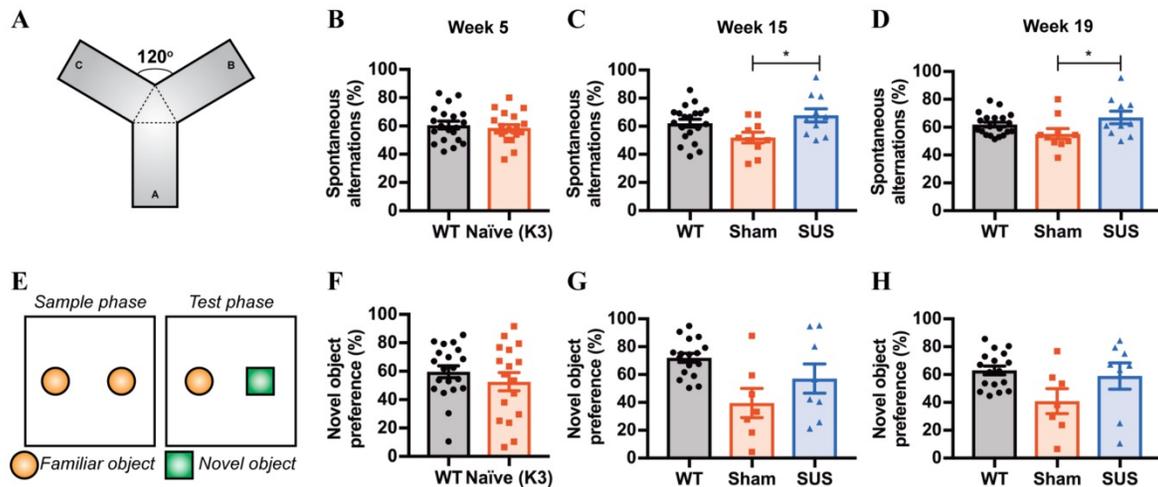
Figure 6. Repeated ultrasound treatments improve memory functions of SUS-treated K3 mice. (A) To test spatial working memory, the sequence of arm entries in the Y-maze was used to measure spontaneous alternation. (B) At week 5, the K3 mice did not show any spatial working memory deficit, performing alternations similar to those of their WT littermates (two-tailed unpaired *t*-test) (n=20 WT and 20 K3 mice). (C) At week 15, and (D) at week 19, the SUS-treated K3 mice performed significantly more spontaneous alternations than the sham group (one-way ANOVA with Tukey's multiple comparison test, *p<0.05) (n=20 WT, 10 sham and 10 SUS-treated mice). (E) Recognition memory was assessed in the NOR paradigm, where the time spent exploring a novel object was used to measure the animals' preference for this object and their memory of a familiar object. (F) At week 5, the K3 mice performed equally as well as WT mice (two-tailed unpaired *t*-test) (n=20 WT and 20 K3 mice). (G, H) At weeks 15 and 19, the SUS-treated animals showed a trend towards exploring the novel object more than the familiar object (60%), although the result failed to reach significance (one-way ANOVA with Tukey's multiple comparison test) (n=17 WT, 7 sham and 8 SUS-treated mice).

pathology, underscoring the validity of low-intensity ultrasound as a potential treatment for Alzheimer's disease and other tauopathies [22].

Here, we show for the first time that low-intensity ultrasound also reduces tau pathology without the need for additional therapeutic agents in the K369I tau transgenic K3 mice, while also improving the motor and potentially memory deficits associated with this strain. We first demonstrated that 15 SUS treatments were safely tolerated by the K3 mice. This is an important finding as a therapeutic effect of ultrasound in humans may require multiple BBB opening sessions over an extended period of time. Prior to the current study, ultrasound alone had not been explored as a therapeutic modality in mice with pronounced tau-mediated motor impairments, nor had longer treatments of the entire brain been explored. In comparison, Olumolade and colleagues conducted biweekly or monthly sonications over 5 months, safely targeting the striatum without observing any adverse effects on the behavior of wild-type mice [38]. We have also analyzed the long-term effects of SUS in aged wild-type mice, using various imaging tools, showing that ultrasound treatment is potentially safe in older animals [39]. Our current study complements these findings regarding the safety of multiple ultrasound treatments, suggesting that by choosing appropriate ultrasound parameters, longer durations of ultrasound treatments for the entire brain are potentially safe.

We had previously highlighted the potential of SUS to deliver an anti-tau antibody fragment to the mouse brain, thereby reducing tau pathology and

rescuing the associated anxiety-like behavior [22]. Although the ultrasound-only control group in that study showed a reduction in tau pathology, it failed to exhibit improvements in anxiety-like behavior over a 4-week regime. This effect was not investigated further as the main aim of the study was to establish ultrasound as a method to deliver antibodies into the brain. In the current study, we have shown that repeated ultrasound treatments can reduce tau hyperphosphorylation in the K3 transgenic mice while also tending to improve associated memory and motor deficits, without the need for a therapeutic agent. Of note, in previous immunization studies with K3 mice, vaccination failed to improve motor functions, despite achieving a reduction in tau pathology [40]. It is important to note that the K3 model of tau pathology is particularly robust, with the mice developing motor deficits as early as 4 weeks of age, whereas memory deficits have previously been reported at 4 months of age [24]. This robust development of pathology and behavioral deficits presents a challenge for ultrasound as a therapeutic strategy; however, in a human setting, a potential treatment could be envisaged at an early and slowly progressing stage of disease.

Under physiological conditions, cytoplasmic proteins are degraded by the ubiquitin-proteasome system (UPS) and the autophagy pathway, with soluble tau being recycled by the proteasome and aggregated tau clearance being attributed to autophagosomal degradation. Ubiquitinated tau has been demonstrated in the filamentous aggregates at synapses in Alzheimer's disease brains, together with

the inhibition of proteasomal subunits, thereby indicating an impairment of the UPS machinery [41]. On the other hand, the accumulation of autophagosomes in Alzheimer's disease suggests a possible impairment of the autophagy pathway [42]. The reduction of hyperphosphorylated tau observed in our study is unlikely to be the result of increased clearance of tau by the UPS, as we did not observe any effect of ultrasound on the ubiquitination of tau. It has to be noted that our study design allowed us to only detect the clearance mechanism which was active at the time when the mice were sacrificed, which means that we cannot rule out the possibility that additional clearance mechanisms were operating at earlier time-points. However, our results clearly demonstrate that autophagy is induced specifically in neurons and not in glia following repeated ultrasound treatment. We observed a reduced mTOR activity in the SUS-treated mice as compared to the sham group. mTOR is a negative regulator of autophagy and has been found to be increased in Alzheimer's disease [43], with associated changes in its downstream substrates suggesting a loss of protein translational control. On the other hand, treatment with the mTOR inhibitor rapamycin has been reported to reduce tau pathology in P301S tau transgenic mice through the induction of autophagy [44]. In our study, we found an increased interaction of tau with autophagosomes, further supporting the idea that pathological tau is cleared by autophagy in response to repeated ultrasound treatments. These results further add to the claim that the induction of autophagy, achieved by either pharmacological interventions using methylene blue, trehalose or rapamycin [25, 44, 45], or by a non-pharmacological approach such as SUS, can reduce tau hyperphosphorylation, leading to functional improvements.

An increasing number of therapies that target various aspects of tauopathies are reaching clinical development, including strategies involving vaccinations targeting both phospho- and pan-tau species [8]. The location and distribution of the various tau species targeted by these antibodies dictates the mechanism by which pathological tau is being cleared. Extracellular tau is mostly removed through microglial phagocytosis of the antibody-tau complex or through the sequestration of extracellular tau so as to inhibit the propagation of tau, whereas intracellular tau is targeted by antibodies that need to be internalized by neurons, facilitating clearance via autophagic and lysosomal pathways of degradation [46]. Although we have shown that repeated ultrasound treatments increase the clearance of tau through autophagy, we do not rule out a potential

role of microglia, as previously reported in the case of amyloid-β clearance [21].

Taken together with previous work [21], our data suggest that SUS has the potential to clear the two prominent Alzheimer's disease pathologies, amyloid-β plaques and tau NFTs, simultaneously, albeit possibly by separate yet partly overlapping mechanisms. Moreover, our findings indicate that repeated treatments with low-intensity ultrasound in the absence of a therapeutic agent may be effective in more generally reducing intracellular protein aggregates, a feature that also characterizes the most prominent movement disorder, Parkinson's disease.

Abbreviations

BBB: blood-brain barrier; NFTs: neurofibrillary tangles; SUS: scanning ultrasound.

Supplementary Material

Supplementary figures.
http://www.thno.org/v09p3754s1.pdf

Competing Interests

The authors have declared that no competing interest exists.

References

1. Spillantini MG, Goedert M. Tau pathology and neurodegeneration. Lancet Neurol. 2013; 12: 609-22.
2. Arendt T, Stieler JT, Holzer M. Tau and tauopathies. Brain Res Bull. 2016; 126: 238-92.
3. De Strooper B, Karran E. The Cellular Phase of Alzheimer's Disease. Cell. 2016; 164: 603-15.
4. Bodea LG, Eckert A, Ittner LM, Piguet O, Götz J. Tau physiology and pathomechanisms in frontotemporal lobar degeneration. J Neurochem. 2016; 138 Suppl 1: 71-94.
5. Tolnay M, Probst A. REVIEW: tau protein pathology in Alzheimer's disease and related disorders. Neuropathol Appl Neurobiol. 1999; 25: 171-87.
6. Goedert M. The ordered assembly of tau is the gain-of-toxic function that causes human tauopathies. Alzheimers Dement. 2016; 12: 1040-50.
7. Li C, Götz J. Somatodendritic accumulation of Tau in Alzheimer's disease is promoted by Fyn-mediated local protein translation. EMBO J. 2017; 36: 3120-38.

8. Li C, Götz J. Tau-based therapies in neurodegeneration: opportunities and challenges. Nat Rev Drug Discov. 2017; 16: 863-83.
9. Pardridge WM. Drug transport across the blood-brain barrier. J Cereb Blood Flow Metab. 2012; 32: 1959-72.
10. Wu SY, Aurup C, Sanchez CS, Grondin J, Zheng W, Kamimura H, et al. Efficient Blood-Brain Barrier Opening in Primates with Neuronavigation-Guided Ultrasound and Real-Time Acoustic Mapping. Sci Rep. 2018; 8: 7978.
11. Lipsman N, Meng Y, Bethune AJ, Huang Y, Lam B, Masellis M, et al. Blood-brain barrier opening in Alzheimer's disease using MR-guided focused ultrasound. Nat Commun. 2018; 9: 2336.
12. Meng Y, Volpini M, Black S, Lozano AM, Hynynen K, Lipsman N. Focused ultrasound as a novel strategy for Alzheimer disease therapeutics. Ann Neurol. 2017; 81: 611-7.
13. Leinenga G, Langton C, Nisbet R, Götz J. Ultrasound treatment of neurological diseases--current and emerging applications. Nat Rev Neurol. 2016; 12: 161-74.
14. Aubry JF, Tanter M. MR-Guided Transcranial Focused Ultrasound. Adv Exp Med Biol. 2016; 880: 97-111.
15. Poon C, McMahon D, Hynynen K. Noninvasive and targeted delivery of therapeutics to the brain using focused ultrasound. Neuropharmacology. 2017; 120: 20-37.
16. Kinoshita M, McDannold N, Jolesz FA, Hynynen K. Noninvasive localized delivery of Herceptin to the mouse brain by MRI-guided focused ultrasound-induced blood-brain barrier disruption. Proc Natl Acad Sci U S A. 2006; 103: 11719-23.
17. Sheikov N, McDannold N, Sharma S, Hynynen K. Effect of focused ultrasound applied with an ultrasound contrast agent on the tight junctional integrity of the brain microvascular endothelium. Ultrasound Med Biol. 2008; 34: 1093-104.
18. Jordao JF, Ayala-Grosso CA, Markham K, Huang Y, Chopra R, McLaurin J, et al. Antibodies targeted to the brain with image-guided focused ultrasound reduces amyloid-beta plaque load in the TgCRND8 mouse model of Alzheimer's disease. PLoS One. 2010; 5: e10549.
19. Jordao JF, Thevenot E, Markham-Coultes K, Scarcelli T, Weng YQ, Xhima K, et al. Amyloid-beta plaque reduction, endogenous antibody delivery and glial activation by brain-targeted, transcranial focused ultrasound. Exp Neurol. 2013; 248: 16-29.
20. Burgess A, Dubey S, Yeung S, Hough O, Eterman N, Aubert I, et al. Alzheimer disease in a mouse model: MR imaging-guided focused ultrasound targeted to the hippocampus opens the blood-brain barrier and improves pathologic abnormalities and behavior. Radiology. 2014; 273: 736-45.
21. Leinenga G, Götz J. Scanning ultrasound removes amyloid-beta and restores memory in an Alzheimer's disease mouse model. Sci Transl Med. 2015; 7: 278ra33.
22. Nisbet RM, Van der Jeugd A, Leinenga G, Evans HT, Janowicz PW, Götz J. Combined effects of scanning ultrasound and a tau-specific single chain antibody in a tau transgenic mouse model. Brain. 2017; 140: 1220-30.
23. Hoglinger GU, Respondek G, Kovacs GG. New classification of tauopathies. Rev Neurol (Paris). 2018.
24. Ittner LM, Fath T, Ke YD, Bi M, van Eersel J, Li KM, et al. Parkinsonism and impaired axonal transport in a mouse model of frontotemporal dementia. Proc Natl Acad Sci U S A. 2008; 105: 15997-6002.
25. Schaeffer V, Lavenir I, Ozcelik S, Tolnay M, Winkler DT, Goedert M. Stimulation of autophagy reduces neurodegeneration in a mouse model of human tauopathy. Brain. 2012; 135: 2169-77.
26. Seip R, Chin CT, Hall CS, Raju BI, Ghanem A, Tiemann K. Targeted ultrasound-mediated delivery of nanoparticles: on the development of a new HIFU-based therapy and imaging device. IEEE Trans Biomed Eng. 2010; 57: 61-70.
27. van Eersel J, Ke YD, Liu X, Delerue F, Kril JJ, Götz J, et al. Sodium selenate mitigates tau pathology, neurodegeneration, and functional deficits in Alzheimer's disease models. Proc Natl Acad Sci U S A. 2010; 107: 13888-93.
28. Brici D, Götz J, Nisbet RM. A Novel Antibody Targeting Tau Phosphorylated at Serine 235 Detects Neurofibrillary Tangles. J Alzheimers Dis. 2018; 61: 899-905.
29. Iqbal K, Liu F, Gong CX. Tau and neurodegenerative disease: the story so far. Nat Rev Neurol. 2016; 12: 15-27.
30. Khanna MR, Kovalevich J, Lee VM, Trojanowski JQ, Brunden KR. Therapeutic strategies for the treatment of tauopathies: Hopes and challenges. Alzheimers Dement. 2016; 12: 1051-65.
31. Leinenga G, Götz J. Safety and Efficacy of Scanning Ultrasound Treatment of Aged APP23 Mice. Front Neurosci. 2018; 12: 55.
32. Lee MJ, Lee JH, Rubinsztein DC. Tau degradation: the ubiquitin-proteasome system versus the autophagy-lysosome system. Prog Neurobiol. 2013; 105: 49-59.
33. Kang R, Zeh HJ, Lotze MT, Tang D. The Beclin 1 network regulates autophagy and apoptosis. Cell Death Differ. 2011; 18: 571-80.
34. Otomo C, Metlagel Z, Takaesu G, Otomo T. Structure of the human ATG12~ATG5 conjugate required for LC3 lipidation in autophagy. Nat Struct Mol Biol. 2013; 20: 59-66.
35. Benito-Cuesta I, Diez H, Ordonez L, Wandosell F. Assessment of Autophagy in Neurons and Brain Tissue. Cells. 2017; 6.
36. Yoshii SR, Mizushima N. Monitoring and Measuring Autophagy. Int J Mol Sci. 2017; 18.
37. Bjorkoy G, Lamark T, Pankiv S, Overvatn A, Brech A, Johansen T. Monitoring autophagic degradation of p62/SQSTM1. Methods Enzymol. 2009; 452: 181-97.
38. Olumolade OO, Wang S, Samiotaki G, Konofagou EE. Longitudinal Motor and Behavioral Assessment of Blood-Brain Barrier Opening with Transcranial Focused Ultrasound. Ultrasound Med Biol. 2016; 42: 2270-82.
39. Blackmore DG, Turpin F, Mohamed AZ, Zong F, Pandit R, Pelekanos M, et al. Multimodal analysis of aged wild-type mice exposed to repeated scanning ultrasound treatments demonstrates long-term safety. Theranostics. 2018; 8: 6233-47.
40. Ittner A, Bertz J, Suh LS, Stevens CH, Götz J, Ittner LM. Tau-targeting passive immunization modulates aspects of pathology in tau transgenic mice. J Neurochem. 2015; 132: 135-45.
41. Tai HC, Serrano-Pozo A, Hashimoto T, Frosch MP, Spires-Jones TL, Hyman BT. The synaptic accumulation of hyperphosphorylated tau oligomers in Alzheimer disease is associated with dysfunction of the ubiquitin-proteasome system. Am J Pathol. 2012; 181: 1426-35.
42. Nixon RA, Wegiel J, Kumar A, Yu WH, Peterhoff C, Cataldo A, et al. Extensive involvement of autophagy in Alzheimer disease: an immuno-electron microscopy study. J Neuropathol Exp Neurol. 2005; 64: 113-22.
43. Li X, Alafuzoff I, Soininen H, Winblad B, Pei JJ. Levels of mTOR and its downstream targets 4E-BP1, eEF2, and eEF2 kinase in relationships with tau in Alzheimer's disease brain. FEBS J. 2005; 272: 4211-20.
44. Ozcelik S, Fraser G, Castets P, Schaeffer V, Skachokova Z, Breu K, et al. Rapamycin attenuates the progression of tau pathology in P301S tau transgenic mice. PLoS One. 2013; 8: e62459.
45. Congdon EE, Wu JW, Myeku N, Figueroa YH, Herman M, Marinec PS, et al. Methylthioninium chloride (methylene blue) induces autophagy and attenuates tauopathy in vitro and in vivo. Autophagy. 2012; 8: 609-22.
46. Sigurdsson EM. Tau Immunotherapy. Neurodegener Dis. 2016; 16: 34-8.